Article

Neuron

Central Gain Restores Auditory Processing following Near-Complete Cochlear Denervation

Highlights

- Normal sound detection persists in the absence of peripheral markers of hearing
- Faster and more complete recovery from cochlear denervation in cortex than midbrain
- Enhanced cortical gain supports features encoded by spike rate, not spike timing
- Recovery is more complete after unilateral denervation than bilateral denervation

Authors

Anna R. Chambers, Jennifer Resnik, Yasheng Yuan, Jonathon P. Whitton, Albert S. Edge, M. Charles Liberman, Daniel B. Polley

Correspondence

polley@meei.harvard.edu

In Brief

Removing 95% of cochlear afferent synapses eliminates sound-evoked brainstem responses and acoustic reflexes, yet sound detection remains normal. Chambers and colleagues describe a cortical amplifier that recovers sound feature representations supported by neural rate-coding, but not precise spike timing.

Chambers et al., 2016, Neuron *89*, 867–879
February 17, 2016
http://dx.doi.org/10.1016/j.neuron.2015.12.041

CellPress

Neuron
Article

Central Gain Restores Auditory Processing following Near-Complete Cochlear Denervation

Anna R. Chambers,[1,4] Jennifer Resnik,[1,2] Yasheng Yuan,[3] Jonathon P. Whitton,[1] Albert S. Edge,[1,2] M. Charles Liberman,[1,2] and Daniel B. Polley[1,2,*]
[1]Eaton-Peabody Laboratories, Massachusetts Eye and Ear Infirmary, Boston, MA 02114, USA
[2]Department of Otolaryngology, Harvard Medical School, Boston, MA 02114, USA
[3]Department of Otolaryngology, Fudan University, Shanghai 200031, China
[4]Present address: Johannes Gutenberg University Mainz, Hanns-Dieter-Hüsch Weg 19, 55128 Mainz, Germany
*Correspondence: polley@meei.harvard.edu
http://dx.doi.org/10.1016/j.neuron.2015.12.041

SUMMARY

Sensory organ damage induces a host of cellular and physiological changes in the periphery and the brain. Here, we show that some aspects of auditory processing recover after profound cochlear denervation due to a progressive, compensatory plasticity at higher stages of the central auditory pathway. Lesioning >95% of cochlear nerve afferent synapses, while sparing hair cells, in adult mice virtually eliminated the auditory brainstem response and acoustic startle reflex, yet tone detection behavior was nearly normal. As sound-evoked responses from the auditory nerve grew progressively weaker following denervation, sound-evoked activity in the cortex—and, to a lesser extent, the midbrain—rebounded or surpassed control levels. Increased central gain supported the recovery of rudimentary sound features encoded by firing rate, but not features encoded by precise spike timing such as modulated noise or speech. These findings underscore the importance of central plasticity in the perceptual sequelae of cochlear hearing impairment.

INTRODUCTION

Neural circuits in the auditory periphery and brainstem feature remarkable biophysical and synaptic specializations that support acoustic feature extraction with temporal precision on the order of tens of microseconds (Lu et al., 2008; Mathews et al., 2010; McGinley et al., 2012). High-fidelity sound representations at early stages of auditory processing are reformatted as abstractions of the source signal in higher centers (Atencio et al., 2012; Pasley et al., 2012; Rabinowitz et al., 2013; Wang et al., 2008). While higher auditory neurons are not equipped to track rapid fluctuations in the acoustic waveform, their synaptic and intrinsic architecture is optimized instead for dynamic, integrative processing that is essential to auditory perception. These emergent higher auditory processes support adapting to complex statistical patterns that unfold over extended timescales (Ayala et al., 2013; Dean et al., 2008; Rabinowitz et al., 2011; Yaron et al., 2012), dynamic shifts in auditory sensitivity to reflect past experience or focused attention (Diamond and Weinberger, 1986; Mesgarani and Chang, 2012) and homeostatic processes that normalize neural activity following abrupt shifts in afferent drive (Auerbach et al., 2014; Qiu et al., 2000; Yang et al., 2011).

The perception of sound is tightly coupled to cortical processing dynamics. These links have primarily been demonstrated in the context of attentive listening (Ding and Simon, 2012; Gutschalk et al., 2008; Mesgarani and Chang, 2012; Zion Golumbic et al., 2013) or adaptive receptive field modulation (Atiani et al., 2009; Froemke et al., 2013). Cochlear damage induces profound changes in the input gain, temporal processing, neural morphology, and excitatory/inhibitory balance of adult cortex that develop in tandem with peripheral pathology (Mowery et al., 2015; Reed et al., 2014; Robertson and Irvine, 1989; Scholl and Wehr, 2008; Tomita et al., 2004; Yang et al., 2011, 2012). However, apart from its role in the generation of tinnitus (Auerbach et al., 2014), central plasticity is not commonly thought to play an essential role in the perceptual sequelae of cochlear hearing loss. Instead, the hallmarks of hearing loss—threshold elevation, reduced frequency resolution, poor discrimination of signals in noise, and compressed loudness growth functions — have traditionally been attributed to changes in cochlear mechanics or the loss of particular cell types in the cochlea or auditory nerve (Moore, 2007). This point of view is necessarily incomplete; a thorough understanding of the biological determinants of hearing loss must reconcile the peripheral pathology with the possibility of additional changes in higher auditory circuits that directly give rise to perception.

Auditory neuropathy spectrum disorder (ANSD) is an enigmatic, recently described neurological disorder in which patients with degeneration of the auditory afferent pathway present with relatively normal cochlear amplification, hearing thresholds, and sound-evoked cortical potentials, but have profound disruptions in the auditory brainstem response (ABR), brainstem acoustic reflexes, and speech reception (Starr et al., 1996). This disorder has been renamed Auditory Neuropathy Dys-synchrony Disorder based on the presumption that these perceptual manifestations must arise from demyelination and dys-synchronization of remaining auditory nerve fibers (Berlin et al., 2010). Here, we introduce a mouse model for ANSD that exhibits the complete spectrum of auditory dysfunction noted in the human condition.

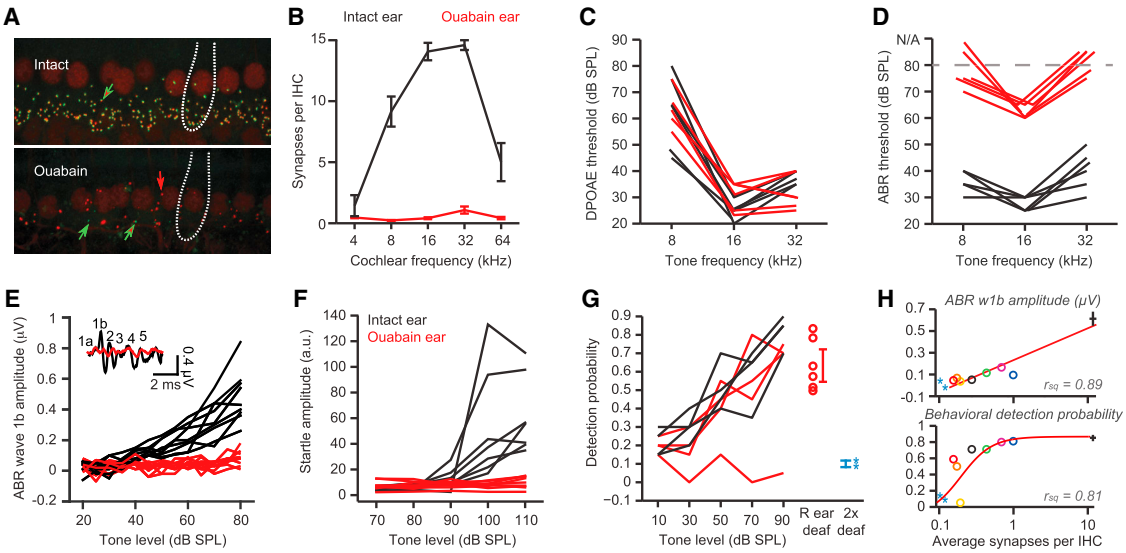

Figure 1. Ouabain Eliminated >95% of Type-I SGN Synapses and Most Indications of Hearing According to Brainstem Activity, yet Tone Audibility Remained Intact

(A) Cochlear histopathology from a control (top) and ouabain-treated (bottom) adult mouse. The juxtaposition of IHC presynaptic ribbons (red) and glutamate postsynaptic receptors (green) indicate a functional synapse (combined red and green arrow). The orphaned ribbons and receptors are indicated by purely red or green arrows, respectively. The IHCs are outlined in white.

(B) Synaptic counts per IHC across the cochlear frequency axis (intact ear, black line: n = 4; ouabain ear, red line: n = 13; F = 377.7; p < 0.01; and repeated-measures ANOVA. The error bars are mean ± SEM).

(C) DPOAE thresholds indicated that hair cell amplification was intact and functional (intact ear versus ouabain ear, n = 8; F = 1.1; p = 0.31; and repeated-measures ANOVA).

(D and E) ABR wave 1b (E, inset) thresholds (D, n = 8, F = 68.8, p < 0.01, and repeated-measures ANOVA) and amplitudes (E, n = 8, F = 28.9, p < 0.01) at 8 kHz reflect the massive loss of nerve fibers.

(F and G) Auditory startle response (F) and tone detection (G) are shown for the same mice (A–E) also using 8 kHz tones. The startle response is eliminated in all mice after ouabain (n = 6, F = 11.1, p < 0.01, and repeated-measures ANOVA) despite normal tone sensitivity in 3/4 mice.

(G) In a different cohort of mice, detection probability at 80–90 dB SPL through the denervated ear is tested with the control ear deafened (red, n = 6) or in mice with 100% elimination of Type-I SGNs in both ears (blue, n = 2) (right). The error bars are mean ± SEM.

(H) 8 kHz ABR w1b amplitude (top) and 8 kHz tone detection probability at 80–90 dB (bottom) is compared to synaptic innervation at the 8 kHz region of the cochlea (individual mice are distinguished by circle color).

In contrast to descriptions based on peripheral synchronization, we show that persistent sound awareness in the face of profound, unremitting peripheral and brainstem dysfunction may be attributed to a plasticity at higher stages of auditory processing. This compensatory plasticity is sufficient to recover rudimentary sound features that can be encoded by variations in overall firing rate but—absent the commensurate recovery of essential brainstem circuits—falls short of supporting the precise representation of temporally complex stimuli. As a final point, we show that central compensation is far more complete following unilateral denervation than bilateral denervation.

RESULTS

Ouabain Decimates Synaptic Innervation of Inner Hair Cells without Affecting Cochlear Amplification

Most forms of sensorineural hearing loss induce an inextricable set of changes in the central auditory pathway and the cochlear transduction and amplification machinery. To better isolate the contribution of central plasticity, we employed a method to selectively eliminate afferent fibers from Type-I spiral ganglion neurons (SGNs) without damaging other types of afferent fibers, efferent fibers, or sensory and non-sensory cells in the organ of Corti. This was achieved with round window application of ouabain, a Na^{2+}/K^{+} ATPase pump inhibitor that, in mice, specifically lesions Type-I SGNs (Lang et al., 2005; Yuan et al., 2014).

Unilateral ouabain treatment reduced the synaptic contacts from Type-I SGNs onto inner hair cells (IHC) from ~10–15 in the untreated ear to less than 1 per IHC across the cochlear frequency axis without affecting the distortion product otoacoustic emission, a measure of outer hair cell amplification (Figures 1A–1C; see corresponding figure legends and Table S1 for statistical results). The functional consequences of cochlear damage are commonly assessed with the ABR, an auditory evoked potential generated by synchronized activity at various stages of peripheral and brainstem processing. ABR thresholds were elevated by approximately 40 dB in the ouabain-treated versus intact ears of individual mice (Figure 1D). Importantly, the input/output function of wave 1b, which is specifically generated by Type-I SGNs, was effectively flat after ouabain treatment (Figure 1E; other tone frequencies and ABR electrode configurations are shown in Figure S1).

Cochlear Denervation Eliminates Tone-Evoked Reflexes without Affecting Tone Perception

We established the hearing status associated with profound SGN loss using two paradigms: the acoustic startle response and an operant detection behavior. Hearing performance was assessed either in the ouabain-treated or intact ear by inserting a custom-shaped foam plug in the untested ear. In an initial series of control experiments we determined that the combination of a properly fitted dense foam ear plug and the high-frequency hearing range of the mouse provided at least 60 dB of attenuation for stimuli used in these tasks (Figures S2B and S2C). The acoustic startle response (ASR) is commonly employed as a behavioral readout of hearing status that is mediated by a brainstem circuit linking cochlear root neurons to spinal motoneurons. As expected from the virtual elimination of ABR wave 1b (Figure 1E), we did not observe any acoustic startle reflex through the ouabain treated ear, although a robust startle response was noted from the intact, untreated ear (Figure 1F, red and black lines, respectively).

The absence of acoustic reflexes and ABR can belie the persistence of robust and sensitive auditory perception in humans on the ANSD spectrum (Starr et al., 1996; Zeng et al., 2005). We therefore measured tone detection with an interrogative behavioral test (rather than a reflexive test) that more closely approximates tone detection measurements used in human subjects. To our surprise, the same mice exhibited nearly identical tone detection behavior in the ouabain-treated and untreated ears, despite having a virtually absent ABR and startle response through the ouabain-treated ear (Figure 1G). As a control for acoustic crosstalk, we trained an additional group of mice in which the untreated ear was mechanically deafened shortly before testing. These mice also showed normal detection probability through the ouabain-treated ear (Figure 1G, red data points n = 6). In another set of mice, we eliminated virtually all SGN synapses onto IHCs in both ears with an extended, bilateral application of ouabain (n = 2). No tone detection behavior was observed in these mice, demonstrating that residual hearing through the ouabain-treated ear was mediated through the tiny fraction of surviving afferent synapses and not, for example, through Type-II fibers or vestibular afferents (Figure 1G, blue data points).

While the amplitude of ABR wave 1b scales logarithmically with the number of Type-I synapses on IHCs ($r2 = 0.89$, $p < 0.01$), the relationship between afferent synapse survival and tone detection behavior is even more steeply non-linear; detection is relatively normal with as little as 3%–4% of the normal afferent innervation, but drops precipitously thereafter (Figure 1H, top versus bottom). These findings suggest that residual tone perception might be supported by persistent auditory processing downstream of the brainstem generators of the ABR and acoustic startle reflex.

A Progressive Recovery of Sound Responsiveness Occurs in the Midbrain and Cortex, but Not in the Auditory Nerve

We established the location and characteristics of persistent auditory function by implanting multichannel electrodes in the central nucleus of the inferior colliculus (IC) and primary auditory cortex (ACtx) contralateral to the ouabain-treated ear (Figures 2A and 2B). This approach allowed us to track recovery of function after nerve injury—or lack thereof—at three stages of processing (nerve, midbrain, and cortex) in individual mice. There were three groups of animals that were tested: (1) control mice in which the left ear was untreated (n = 3) or subjected to sham treatment (n = 2; sterile water application at the round window), (2) a short-term recovery group in which the left ear was treated with ouabain 7 days prior (n = 5), and (3) a long-term recovery group in which the left ear had been treated with ouabain 30 days prior (n = 5; Figure 2C). Multiunit and single unit activity was recorded simultaneously from the IC and ACtx of awake, passively listening animals. In each recording, the untreated right ear (ipsilateral to the recording electrodes) was plugged and sound stimuli were delivered from a speaker opposing the contralateral ear. Note that for all neurophysiology experiments, a double earplug control recording was performed immediately after each unilateral stimulation experiment (Figures S2E–S2G). If acoustic crosstalk was suggested by a persistence of responsiveness after bilateral earplugging, data from those sites were excluded from further analysis (37/728 recording sites).

Ouabain eliminates most SGNs within minutes of application followed by a gradual loss of remaining synapses over subsequent months (Yuan et al., 2014). Accordingly, we observed a marked drop in the wave 1b growth function between controls and 7 days postouabain, that was eliminated altogether by 30 days (Figures 2D and 2G). Higher brain regions showed the opposite trend. We averaged across all unit recordings, both tone-responsive and unresponsive, to provide the most direct basis of comparison to the ABR. In the IC, tone-evoked growth functions from the treated ear increased from 7 to 30 days, but did not recover to control levels (Figures 2E and 2H). Simultaneously recorded ACtx activity revealed persistent responses at 7 days that recovered to levels even greater than control responses by 30 days (Figures 2F and 2I).

These findings highlight an increased central gain that compensates for diminished afferent input (Qiu et al., 2000; Schuknecht and Woellner, 1953; Wake et al., 1996). Compensatory plasticity at the level of the cortex may provide a parsimonious explanation for why mice—like humans on the ANSD spectrum—can exhibit normal tone detection despite the absence of an ABR or acoustic reflexes. Psychophysical studies in ANSD subjects have described relatively normal thresholds for sound intensity discrimination, yet major impairments in the perception of temporal features such as interaural time differences, gaps in noise, and speech (Zeng et al., 2005). We propose that this perceptual dichotomy can be explained by an increased central gain that reinstates coding for basic sound features represented by variations in overall spike rate, but is insufficient for (or perhaps even detrimental to) the recovery of temporally complex feature representations that rely on precise spike timing.

Central Gain Progressively Restores the Representation of Sound Level and Frequency after Cochlear Denervation

To test this hypothesis, we explored whether the increased central gain noted between 7 and 30 days was sufficient to restore a neural firing rate code for intensity and tone frequency. Rate-level functions for each sound-responsive site were analyzed

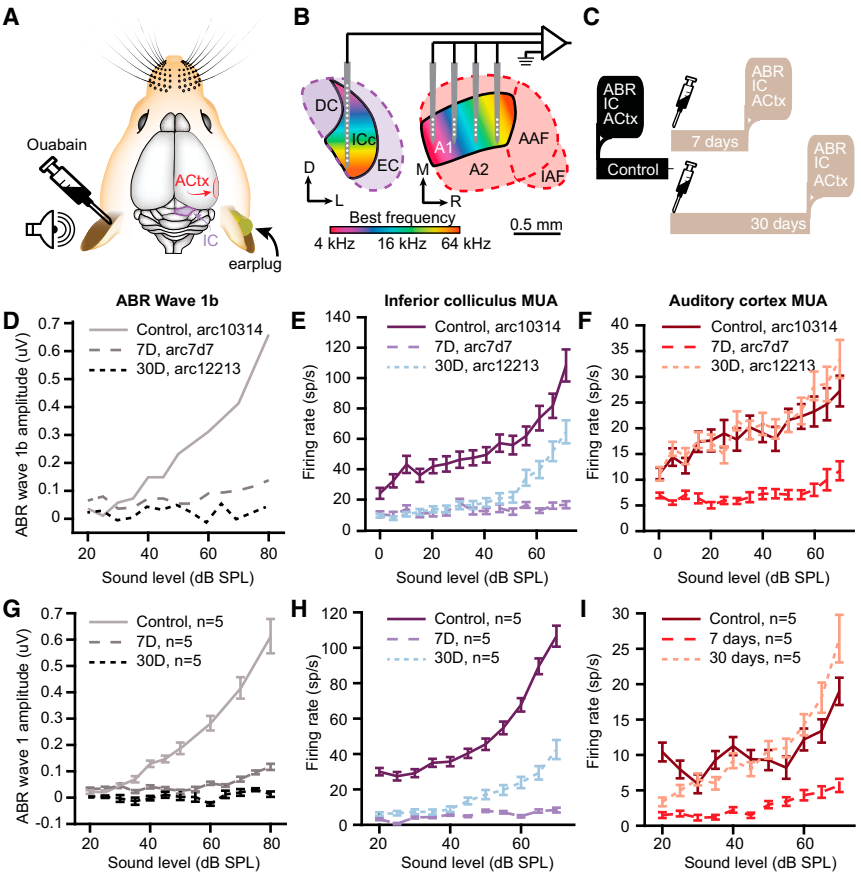

Figure 2. Tone Sensitivity at Higher Stations of Auditory Processing Grows as the Peripheral Response Fades

(A and B) 16 channel silicon probes were chronically implanted in the central nucleus of the IC and the primary ACtx of adult animals with or without ouabain-mediated denervation of the contralateral ear.

(C) Schematic of experimental and control groups. The control animals underwent sham (sterile water applied at the round window) or no treatment, while unilaterally ouabain-treated mice were implanted 7 days or 30 days posttreatment.

(D–F) Example pure tone-elicited growth functions from ABR wave 1 (D), all IC multiunit recordings (E), and all ACtx multiunit recordings (F), measured from an individual mouse in each group (animal ID provided in the legend).

(G) Mean ABR wave 1 pure tone growth functions, ($F(2) = 52.0$, $p < 0.01$, and between groups ANOVA), and population spiking growth functions measured from all recording sites, whether tone-responsive or not, from IC (H, n = 319 sites, $F(2) = 171.5$, $p < 0.01$, and between groups ANOVA) and ACtx (I, n = 298 sites, $F(2) = 19.2$, $p < 0.01$, and between groups ANOVA). The error bars represent SEM.

(broadband noise stimulus, 4–64 kHz, 100 ms in duration, 0–80 dB SPL, and 5 dB steps; Figures 3A and 3B). Thresholds were substantially elevated at 7 days, but recovered by approximately 20 dB by 30 days in both brain areas. Threshold shifts were significantly less pronounced overall in ACtx than IC (Figure 3C). Sound-evoked IC spiking remained depressed after cochlear denervation, even after 30 days (Figure 3D). In ACtx, however, the firing-rate growth function slope was significantly steeper after cochlear denervation, such that the incremental change in spiking per incremental step in SPL was increased at both 7 and 30 days compared to controls, a hallmark of enhanced gain. Similar effects were noted in recordings of isolated single units (Figure S3). Changes in sound-evoked firing rate were not accompanied by significant differences in spontaneous firing rate relative to control (data not shown, unpaired t tests, and $p > 0.05$ after Bonferroni correction for multiple comparisons).

To understand whether changes in the neural representation of sound level amounted to a change in stimulus coding accuracy, we used a PSTH-based classifier (see Experimental Procedures) to decode sound level from single trials of ensemble activity in the IC and ACtx. Confusion matrices depict the mean assignment of stimulus identity based on firing patterns from IC and ACtx units, where correct classification falls along the upward diagonal (20 units per ensemble, Figures 3E–3G, IC, and 3I–3K, ACtx). The mean probability of correct classification is plotted separately for IC and ACtx (Figures 3H and 3L, respectively). Sound-level classification is profoundly disrupted 7 days after ouabain, particularly at low sound levels (Figures 3F and 3J). We observed a near-complete recovery of sound level decoding accuracy by 30 days. In the IC, decoding accuracy at high sound levels matched controls, while lower levels (<50 dB SPL) remained modestly reduced (Figure 3H). Remarkably, sound level classification in ACtx was significantly more accurate across the full range of sound levels 30 days after cochlear denervation compared to control recordings (Figure 3L). This can be attributed to a greater dispersion of cortical thresholds at 30 days compared to control (SD of thresholds = 19.78 and 11.47, respectively, Figure 3C) and steeper growth in firing rate per unit change in sound level (Figure 3D).

To investigate whether recovery extended to other sound features represented by overall changes in firing rate, we compared pure tone frequency response areas (FRAs) in tone-responsive IC and ACtx sites 7 and 30 days after contralateral denervation (0–70 dB SPL, 4–64 kHz in 0.15 octave increments; Figures 4A–4D). Frequency response functions were then reconstructed from a 10 dB range surrounding the preferred sound level from each FRA (Figures 4E and 4F). The robustness of frequency tuning was assessed with a neural d' metric (see Experimental Procedures; Figures 4G and 4H).

In control recordings, tone-evoked multiunit activity was robust, low threshold, and well defined (Figure 4A). Frequency tuning was virtually absent 7 days after cochlear denervation in the IC, but had partially recovered to control levels by 30 days (Figures 4B, 4E, and 4G). By contrast, ACtx frequency tuning was robust 7 days after ouabain. By 30 days, tone-evoked responses were significantly greater than controls, while still

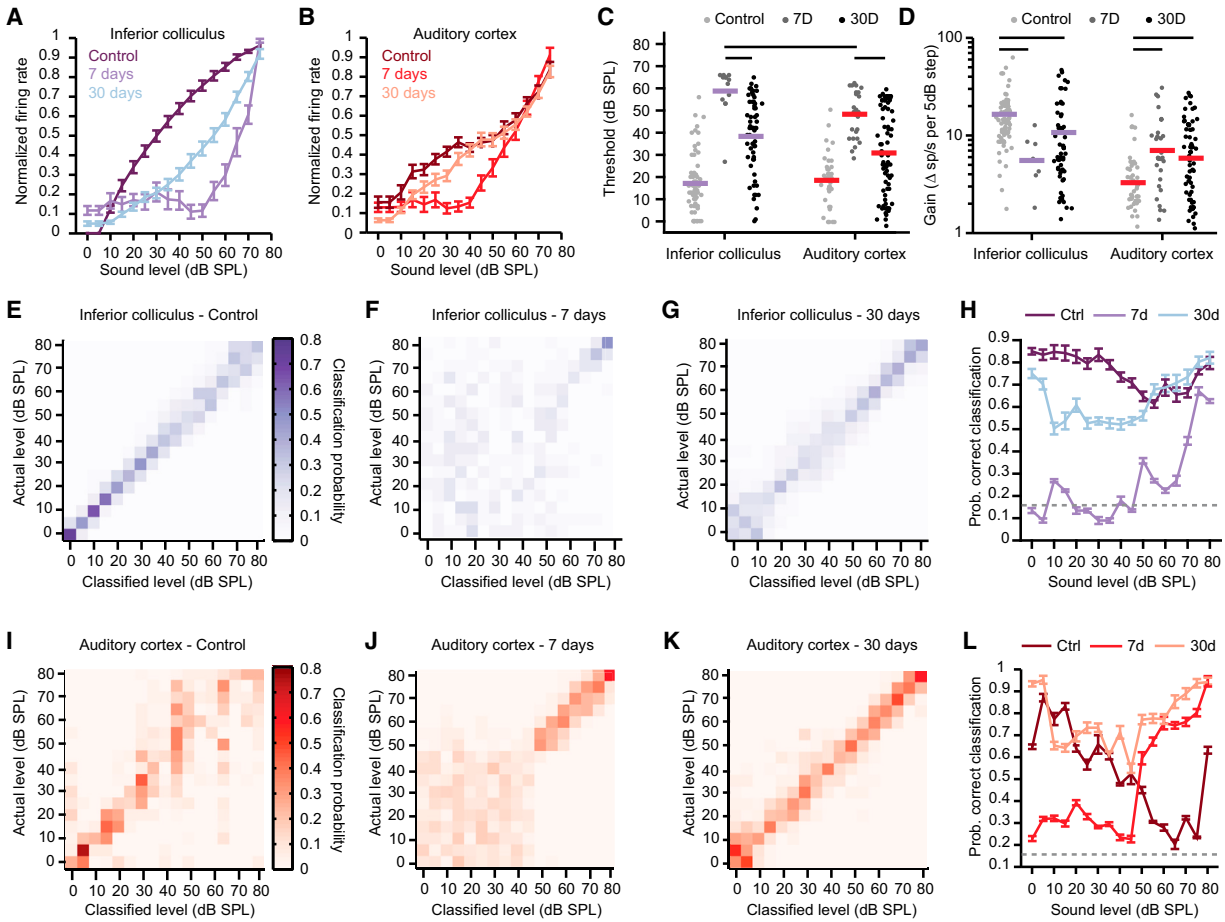

Figure 3. Increased Central Gain Fully Restored Sound Level Coding in ACtx, with Partial Recovery in IC

Analysis for this and all subsequent figures are limited to recording sites with significant sound-evoked activity. ANOVA with post hoc pairwise comparisons are used for testing statistical significance.

(A and B) Normalized firing rate evoked by noise bursts of varying level for IC (A) and ACtx (B) reveal significant recovery from 7 to 30 days, relative to control (ANOVA main effects for group; IC: $F(2) = 56.01$, $p < 0.01$ and ACtx: $F(2) = 13.29$, $p < 0.01$).

(C) Response thresholds at 7 versus 30 days significantly decreased in both brain areas.

(D) Gain can be quantified as the amount of firing rate change per fixed increment of stimulus input, assessed here in non-normalized units of spikes/sec per 5 dB increment of sound level within the initial growth phase of each rate-level function.

(E–G and I–K) Confusion matrices for single trial PSTH-based classification of sound level by IC sites in control (E), 7 day (F), and 30 day (G) postouabain groups. The classification was performed with ensembles of 20 sites, chosen with replacement over 50 repetitions.

(H) Mean probability of veridical classification with IC sites (the diagonal of the confusion matrices ± 5 dB) across sound level for control, 7 day, and 30 day postouabain groups. The dashed gray lines represent chance classification.

(I–K) Confusion matrices for sound level classification with ACtx sites.

(L) Mean probability of correct classification for ACtx sites. The horizontal lines indicate significant differences after unpaired t tests, corrected for multiple comparisons ($p < 0.05$). The error bars represent SEM.

maintaining a clearly defined single-peaked tuning profile (Figures 4D and 4F). Although FRA tuning quality never fully recovered to control levels in the IC, FRA quality in ACtx remained at control levels at both recovery times (Figure 4H). Similar effects were noted in recordings of single units (Figure S4).

Temporal Coding Is Persistently Impaired after Cochlear Neuropathy

Increased central gain, particularly in ACtx, was sufficient to restore basic neural and perhaps perceptual (Figures 1G and 1H) sensitivity to sound, which is reminiscent of audibility and intensity discrimination that is preserved in ANSD patients (Zeng et al., 2005). More complex features, such as temporal fluctuations in the sound pressure envelope, depend on essential processing from peripheral and brainstem circuits that may suffer the brunt of denervation without reaping the benefits of the compensatory plasticity observed at higher processing stations. We therefore turned our attention to temporal decoding accuracy after cochlear afferent denervation using trains of broadband chirp stimuli.

In control recordings, IC unit spiking was synchronized throughout chirp trains with minimal jitter in spike timing

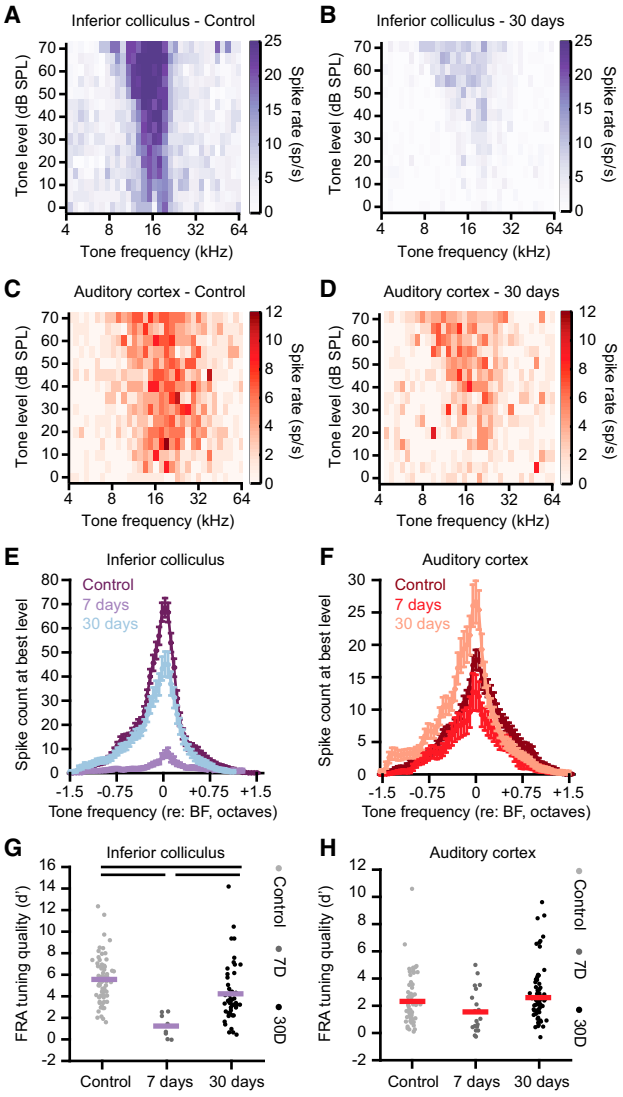

Figure 4. Cochlear Denervation Induces a Short-Term Loss of Frequency Tuning in IC, but Not ACtx

(A–D) FRAs from representative IC (A and B) and ACtx (C and D) recording sites in control or 30 day mice.

(E and F) Mean frequency response functions are derived from the most effective sound level and centered on the best frequency (BF) for all tone-responsive recording sites. In the IC (E), response magnitude at BF is significantly greater at 30 days postouabain compared to 7 days ($p < 0.005$), but is still significantly lower than that observed in the control group ($p < 0.001$). Conversely, in the ACtx (F), tone-evoked responses in the 7 day group were not significantly suppressed compared to control ($p = 0.6$), while peak responses in the 30 day group were significantly higher than control ($p < 0.05$).

(G and H) FRA quality was assessed using a d-prime metric, which quantifies the separability of firing rate distributions drawn from frequencies within versus outside the receptive field boundary (see Supplemental Information). In the IC (G), d-prime values were significantly lower at 7 days compared to control. They were significantly higher in the 30 day group, but did not recover to control levels. In the ACtx (H), d-prime values were not significantly different across groups. Between groups ANOVA was used to test statistical significance. The horizontal lines above the scatter plots indicate pairwise statistical significance after correcting for multiple comparisons. See Table S1 for complete reports on each statistical test. The error bars represent SEM.

(Figure 5A). After cochlear denervation, first spike variability significantly increased across recovery time in IC units, while in the ACtx, where spiking was non-synchronized and relatively imprecise to begin with, variability was not significantly changed any time after cochlear denervation (Figure 5B). Chirp train synchronization was quantified as the cycle-by-cycle vector strength, a term that uses a range of −1 to 1 to indicate the precision and the reliability with which spikes were aligned to each cycle of the stimulus (Yin et al., 2011). IC units in control mice synchronized to chirp rates up to ~100 Hz. Chirp train synchronization did not recover to control levels after either 7 or 30 days of recovery (Figure 5C).

At higher stages of central processing, temporal modulation can be represented either by synchronized responses (a spike timing code) or non-synchronized responses (a spike rate code) (Wang et al., 2008). If central gain can compensate for coding schemes based on rate, but not timing, we would predict a more extreme deficit in encoding pulse trains with fine temporal resolution. To test this hypothesis, we trained the PSTH-based decoder to classify chirp rate from single-trial spiking activity, while explicitly varying the temporal bin and ensemble sizes. In control recordings, IC units can optimally decode stimulus modulation rate with small ensembles and precise spike timing (Figure 5D). At 1 week after cochlear denervation, classification is at chance with all coding schemes. By 30 days, modulation-rate classification remained impaired by as much as 40% with small ensembles and fine temporal resolution, yet accuracy was restored nearly to control levels when chirp train frequency was decoded with coarse resolution across larger ensembles (Figures 5D and 5E). In ACtx, the distribution of spikes over time (i.e., the PSTH) provided comparatively little information about chirp rate (Figures 5D and 5F).

Cochlear Neuropathy Degrades Neural Coding and Discrimination of Speech Sounds

One of the distinguishing features of ANSD is that patients can hear speech without understanding it (Berlin et al., 2010; Starr et al., 1996; Zeng et al., 2005). We propose that this perceptual dichotomy is consistent with a central gain process that can restore spike rate codes, but not spike timing codes. While precisely timed encoding of chirp trains was clearly disrupted after ouabain treatment, we sought to test this hypothesis more directly using broadband, temporally complex, and naturalistic stimuli, while avoiding potential confounds associated with behaviorally relevant conspecific vocalizations. Therefore, we investigated the neural encoding of human speech tokens in ouabain-treated mice.

Consonant-vowel-consonant combinations were digitally resynthesized to span the mouse hearing range without distorting the spectrotemporal envelope of the source signal (Figure 6A). Speech tokens evoked strong responses from IC and ACtx units before and 30 days after ouabain, but not at 7 days (Figure 6A, right). We presented 12 speech tokens that varied by vowel, place of articulation (POA), and voice onset timing (VOT; Figure 6B).

Neural decoding of speech tokens was determined from PSTHs binned at temporal resolutions spanning 1–100 ms. Overall performance improved between 7 and 30 days in the IC,

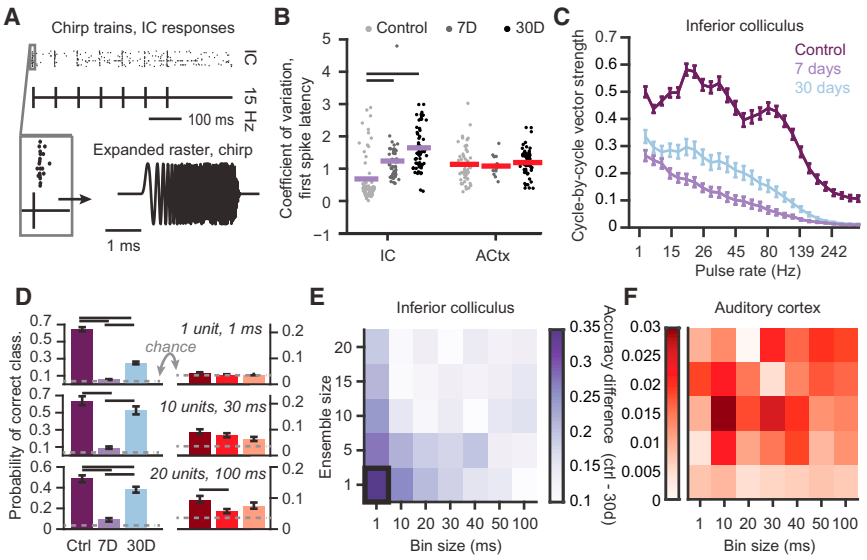

Figure 5. Cochlear Denervation Irreversibly Disrupts Precise Temporal Decoding of Modulation Rate

(A) Trains of 1 ms broadband chirp stimuli (top, one chirp shown in expanded view at bottom) were presented at 20 dB above chip response threshold for each recording site, while unit responses (top, raster to initial chirp shown in expanded view at bottom) were recorded from IC or ACtx.

(B) The coefficient of variation of the first spike latency to a single chirp was measured in both brain areas. In the IC, the first spike latency in the 7 days and 30 days group were significantly elevated compared to controls (post hoc pairwise tests, $p < 0.01$ for each comparison after correcting for multiple comparisons), but not from each other (post hoc pairwise test, $p = 0.29$).

(C) Cycle-by-cycle vector strength, a metric of synchronization, was calculated for IC only, as ACtx exhibited only asynchronous responses to chirp trains in all conditions. The synchronization was significantly impaired relative to control at both the 7 days and 30 days time points.

(D) Mean probability of correct classification averaged across all pulse rates for various combinations of bin size and ensemble size. Note the difference in y axis scaling for IC and ACtx. The horizontal lines above the bar plots indicate significant differences after pairwise tests, corrected for multiple comparisons. The broken horizontal lines indicate the probability of correct classification by chance.

(E and F) Ensemble classification in IC and ACtx for various ensemble sizes and PSTH time bins. The color scale represents control mean classification minus 30 days mean classification, therefore positive values indicate a persistent decoding deficit at 30 days. Note the difference in color axis scaling between IC and ACtx. Between groups ANOVA was used to test the statistical significance. The error bars represent SEM.

except at 1 ms resolution, which was nearly optimal for speech decoding in control recordings (Figure 6C). In ACtx, persistent deficits in speech decoding were observed 30 days after ouabain treatment, specifically when spike trains were binned with finer temporal resolution (Figure 6D), indicating that the same compensatory plasticity that improved level and frequency encoding could not completely salvage the cortical representation of speech tokens. Similar effects were noted in recordings of single units (Figure S5).

We constructed confusion matrices for speech classification from ensembles of IC (Figures 6E–6G) and ACtx units (Figures 6I–6K) using the optimal temporal bin size determined for each brain area and experimental group. Word order for confusion matrices matches the linguistic schematic in Figure 6B, therefore error patterns for neighboring words indicate a concordance between human phonetic and mouse neuronal categorizations. To investigate this further, classification was broken down into correct assignment versus erroneous classification to a word that differed according to POA, VOT, vowel, or "Other", a word varying in more than one of the previous categories (Figures 6H and 6L). At 30 days after ouabain, a disproportionately high number of classification errors were attributed to POA or VOT, while vowel confusion remained relatively low. This suggests that more errors were made resolving the rapid temporal fluctuations that determine consonant identity, rather than the spectral distinctions between vowels.

Compensatory Gain Enhancement Is Competitive, Not Cooperative

In order to test whether plasticity after cochlear denervation reflects a global, cooperative process or an input-specific competitive process, we compared the contralateral and ipsilateral ear frequency tuning functions for individual recording sites (Figure 7A). As expected, we observed a contralateral bias in control IC and ACtx units (Figure 7B). Even though responses to the denervated ear were stronger in ACtx than IC in all mice 7 days after denervation, the aural bias in frequency tuning had shifted to the intact (ipsilateral) ear in nearly every recording site (Figure 7C). Individual differences emerged 30 days after ouabain treatment. Strong contralateral bias was restored in two mice, a balanced representation was noted in arc121713, while all units maintained an ipsilateral bias in arc12113 (Figure 7D). The direction of plasticity—irreversible ipsilateral takeover versus progressive contralateral recovery—bore no obvious relationship to cochlear synaptic survival (synapses per IHC listed in gray).

Increased central gain observed at 30 days could be a heterosynaptic, cooperative plasticity process that would scale up responses to all afferent inputs impinging upon IC or ACtx units, including the unmanipulated ipsilateral ear. Alternatively, inputs from the ipsilateral ear could compete for representational dominance with the denervated contralateral ear, thereby thwarting its recovery of function. As evidenced by the cumulative probability distribution plots of peak spike counts in control and ouabain-treated animals (Figure 7E), contralateral and ipsilateral response magnitudes were modulated in a "push pull" fashion over time, implicating a competitive plasticity whereby units display enhanced responsiveness is input specific.

Contra/ipsi bias is summarized in Figure 7F, where the areas under the tuning functions for each single site were subtracted from each other such that resultant negative values indicated ipsilateral bias, while positive values indicated contralateral

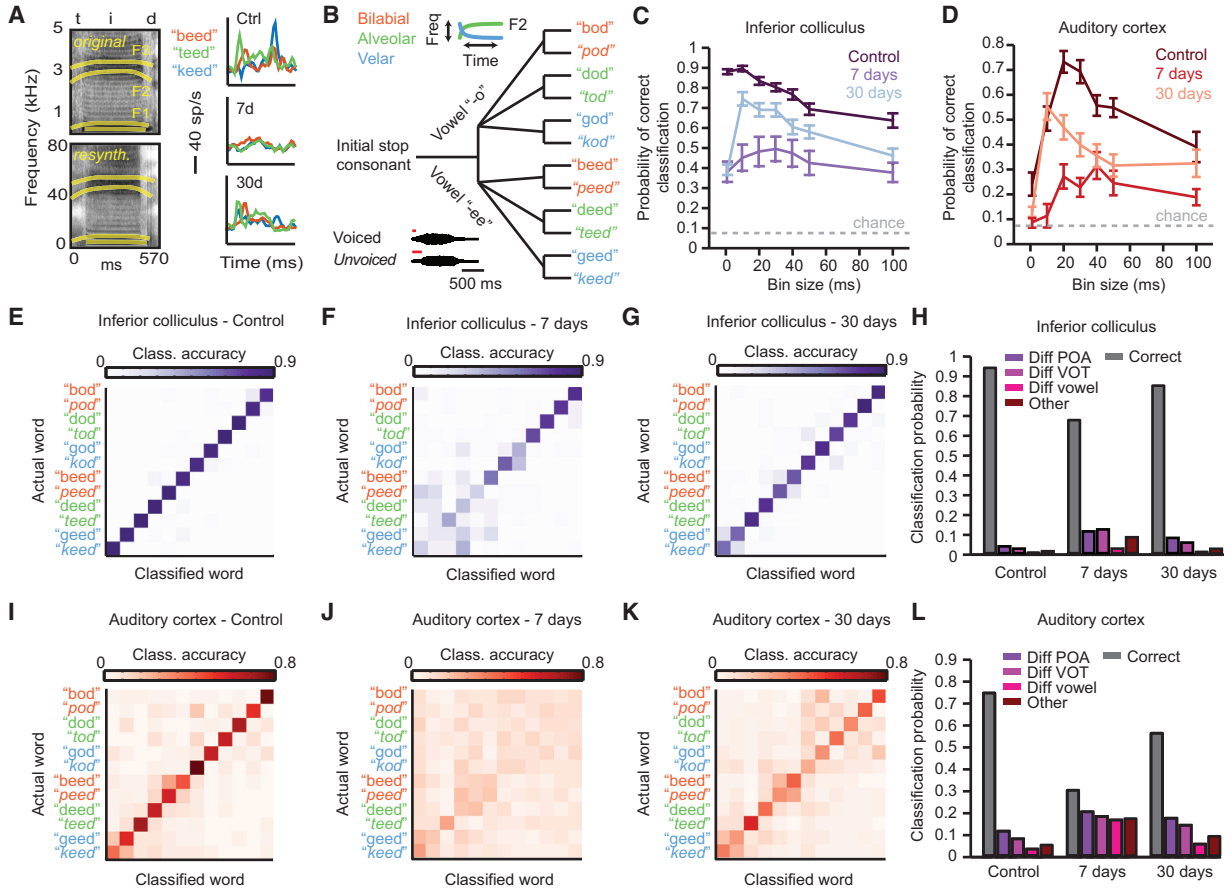

Figure 6. Midbrain and Cortical Coding of Speech Tokens Is Persistently Impaired after Ouabain Treatment

(A) Left: spectrograms of an English speech token in its original form (top) and resynthesized for mouse hearing (bottom). Right: example PSTHs from representative ensembles of ten recording sites taken in control (top), 7 days postouabain (middle), and 30 days postouabain (bottom) conditions). The scale bar shows the y axis firing rate scale for PSTHs. The color of PSTH indicates the word identity. Although speech tokens evoke significant activity in the 30 day condition, PSTHs from various words are less distinguishable.

(B) Phonetic taxonomy for speech tokens, separated into vowel category, POA (color, inset shows formant transitions for two tokens with different places of articulation), and voicing (italics, inset shows example amplitude envelope for a voiced versus unvoiced consonant).

(C and D) Mean probability of veridical speech token classification from single trials of ensemble spiking in IC (C) and ACtx (D) using PSTH bin sizes ranging from 1 ms to 100 ms. In IC, the classification performance is significantly impaired after ouabain treatment ($F(2) = 16.8$, $p < 0.01$). Although there is a trend for improvement between 7 and 30 days posttreatment for bin sizes larger than 1 ms, this is not significant ($p = 0.06$). The significant impairment is also seen in ACtx after ouabain treatment ($F(2) = 27.16$, $p < 0.01$). From 7 to 30 days posttreatment, the classification performance significantly improves, ($p < 0.01$), but not to the level of control ($p < 0.01$).

(E–G) Confusion matrices showing mean ensemble classification for IC recordings using the optimal bin size in control (E), 7 days postouabain (F), and 30 days postouabain (G) conditions.

(H) Correct and erroneous classification probabilities.

(I–L) Same as (E)–(H), but for ACtx ensembles. The classification errors persist in ACtx at 30 days, even at the optimal bin size, particularly for tokens that differ by POA or VOT. Between groups ANOVA was used to test the statistical significance. The error bars represent SEM.

bias. The overall shift from contralateral bias in the control group, to initial ipsilateral bias 7 days after ouabain, and finally a return toward contralateral bias after 30 days, further highlights the dynamic, bidirectional nature of plasticity in the adult cortex and midbrain after peripheral denervation (Cheung et al., 2009).

Signaling from an Intact Ear Facilitates Recovery of Function

The competitive interaction between the contralateral and ipsilateral ears suggested that greater recovery of function might be possible if the ipsilateral ear was also denervated, so as to eliminate its competitive advantage. Indeed, ongoing signaling from an intact ear or ipsilateral skin surface can exaggerate response depression and impede the proper integration and plasticity of reinstated contralateral sensory representations (Glazewski et al., 2007; Kral et al., 2013). On the other hand, more extensive peripheral deafferentation in adult animals can silence the cortex to the point where only very limited reorganization is observed, suggesting that recovery of function would be less robust if both ears were denervated (Keck et al., 2008;

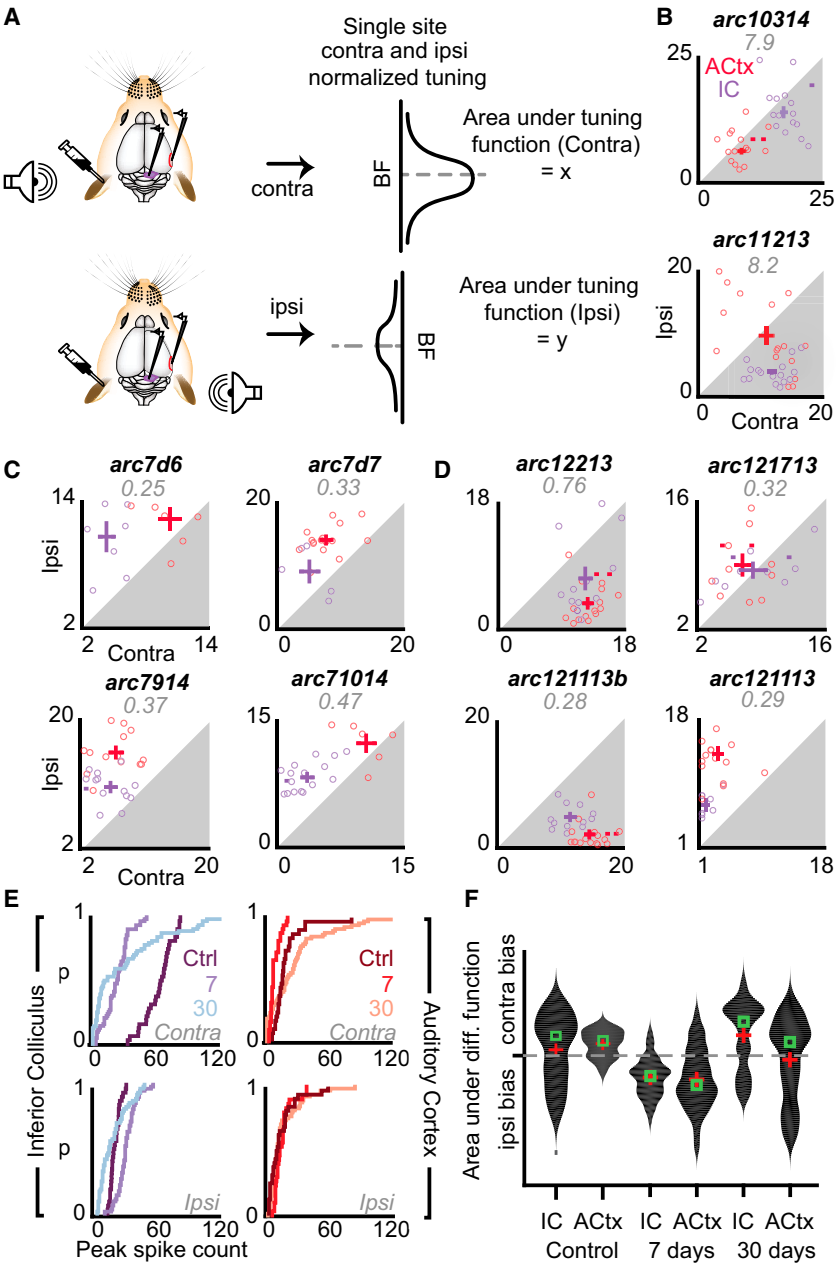

Figure 7. Dynamic Switches in Representational Dominance between the Denervated and Intact Ears

(A) Unilaterally, ouabain-treated animals were fitted with an earplug in either the control or treated ear as sound stimuli were presented to the unplugged ear. The recordings were performed in the IC and ACtx, contralateral to the treated ear, and ipsilateral to the control ear. The stimuli were pure tones from 4–64 kHz in frequency and 0–70 dB in level. The normalized frequency response functions at best level were calculated at significantly responsive (through either ear) recording sites for the ipsilateral (intact ear) and contralateral (ouabain-treated ear) stimulation conditions. The integral of each tuning function was calculated using a trapezoidal approximation and plotted for each site with Contra on the x axis and Ipsi on the y axis.

(B) Ipsi versus Contra tuning function area from the IC and ACtx of two control animals (animal ID indicated in black text and gray italic text indicates the average number of synapses per IHC as revealed by cochlear histopathology). The frequency response functions tend to have a contralateral bias, as evidenced by the mean for each brain area lying below the diagonal. The bidirectional error bars (thick lines) reflect the SEM.

(C) Data from four animals recorded 7 days after ouabain treatment. Having lost a significant amount of input from the normally dominant contralateral ear, the multiunit sites show a bias toward the intact, ipsilateral ear, particularly in the IC recordings.

(D) Data from four animals tested at 30 days after ouabain treatment. The ipsilateral dominance persists in two mice (arc121113 and arc121713), while other mice have reverted to contralateral bias (arc12213 and 121113b).

(E) Cumulative probability distribution of peak spike counts from contralateral (top row) and ipsilateral (bottom row) recording sites in IC (left column) and ACtx (right column). The bidirectional modulation of spike rates is evidenced by the extension of the spike count range to above and below control levels after 30 days.

(F) Distribution plots of the area of the difference function (contra - ipsi) for control, 7 day, and 30 day postouabain conditions. The ipsilateral tuning functions are negative. The mean and median are indicated by red crosses and green squares, respectively. The error bars represent SEM.

Merzenich et al., 1984; Robertson and Irvine, 1989). To address these competing hypotheses, we implanted tetrodes into the ACtx of an additional cohort of mice that underwent bilateral ouabain treatment (n = 6; Figures 8A and 8B). Tetrode recordings allowed us to track the loss and recovery of single unit spike rates over time from a single brain area, rather than comparing cortical and midbrain recovery at specific time points (Figure 8C).

Sound-evoked activity in the auditory nerve was effectively abolished in both ears, as assessed by wave 1b of the ABR (Figure 8D). Sound-evoked spiking from the contralateral ear was abolished 7 days after binaural ouabain, but partially recovered by 30 days, albeit to a far lesser degree than was observed after unilateral ouabain (compare Figures 8E–8G with Figure 2I). Input gain was depressed at 7 days, but then returned to predenervation levels by 30 days, in contrast to elevated gain at both time points with unilateral denervation (compare Figure 8H with Figure 3D). Sound level decoding after bilateral denervation was completely eliminated at 7 days with only modest recovery by 30 days, in contrast to the partial loss at 7 days and supranormal decoding at 30 days after monaural denervation (compare Figures 8I–8L with Figures 3I–3L). These findings suggest that the presence of ongoing signaling from the intact ipsilateral ear helps, rather than hinders, the eventual recovery of function from the denervated, contralateral ear.

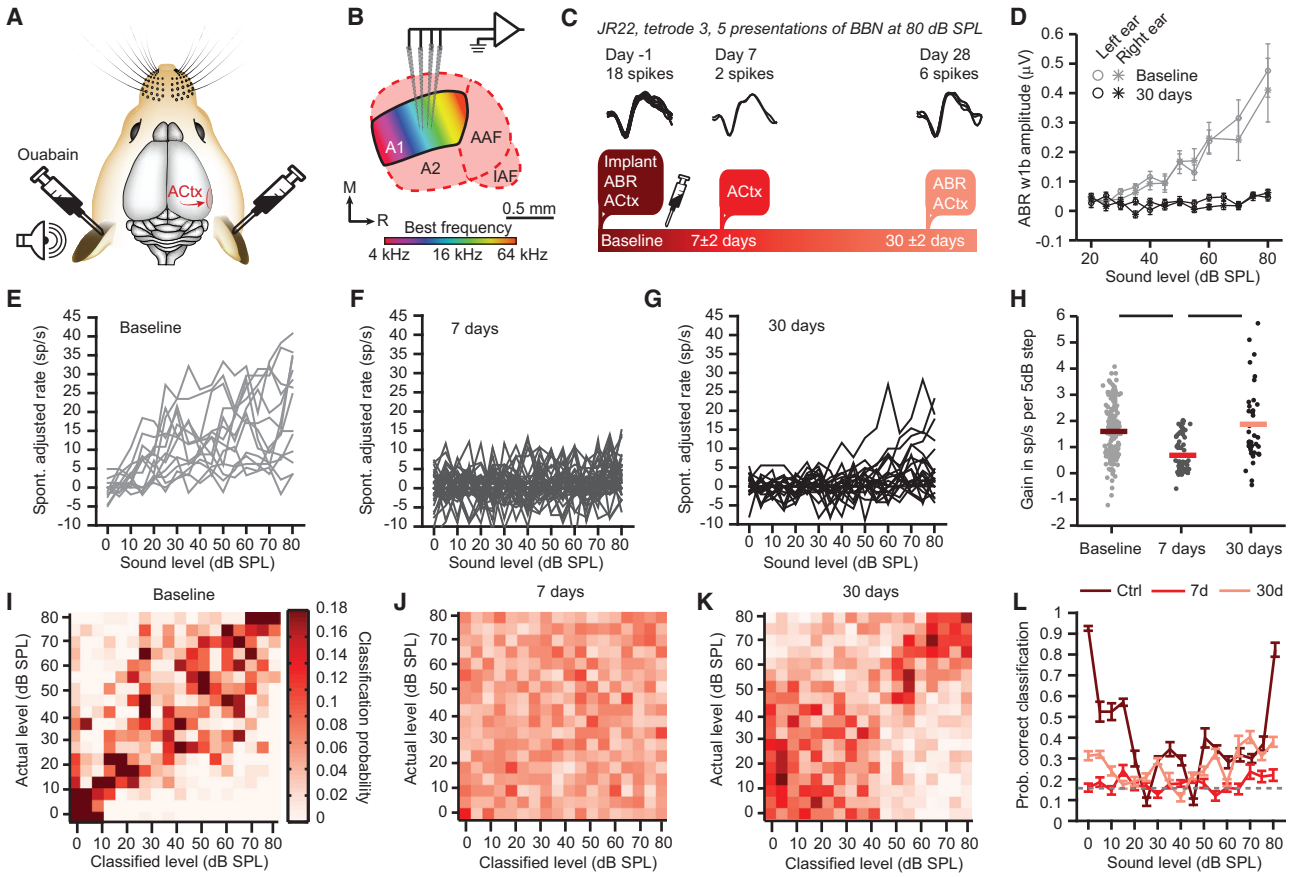

Figure 8. Comparatively Modest Cortical Recovery following Bilateral Cochlear Denervation

In this series of experiments, ouabain was applied bilaterally (A and B) and long-term recording of single units (n = 82 units from six mice) in the right primary ACtx was achieved with four implanted tetrodes.

(C) With this approach, we could record single unit activity from fixed points in ACtx for several days prior to bilateral ouabain application and then again at the 7 day and 30 day time points. We provide an example of all spike waveforms recorded during five trials of a 100 ms noise token presented at 80 dB SPL from a single tetrode wire over a 30 day period from one mouse.

(D) The ABR w1b amplitude growth function is flat for both ears, indicating a massive, bilateral loss of cochlear nerve fibers.

(E–H) Noise-evoked spike rate as a function of SPL after first correcting for prestimulus spontaneous firing rate for all single units recorded either before ouabain application (E) or 7 days (F) and 30 days (G) following oubain application. The modest recovery of sound-evoked firing rate was observed along with a transient loss and subsequent recovery of normative response gain (H).

(I–K) Confusion matrices for sound level classification based on ensembles of 13 ACtx units.

(L) Mean probability of correct classification for ACtx sites. The dashed gray line represents chance classification. The horizontal lines indicate the significant differences after unpaired t tests, corrected for multiple comparisons ($p < 0.05$). The error bars represent SEM.

DISCUSSION

Here, we report that profound cochlear neuropathy nearly eliminated the ABR and startle reflex, but left otoacoustic emissions and behavioral tone detection largely intact (Figure 1). Whereas tone-evoked responses from the auditory nerve became progressively weaker after ouabain, tone-evoked activity from ACtx rebounded to the point where it was even greater than control levels (Figure 2). The recovery of spike rate-based decoding of sound level (Figure 3) and frequency (Figure 4) was more rapid and complete in ACtx than IC. By contrast, trial-by-trial reliability, spike timing precision, and decoding accuracy for pulse trains and speech tokens did not recover to the same degree (Figures 5 and 6). We found that recovery of function appeared to be governed by a competitive plasticity process requiring the denervated ear to "earn back" the territory appropriated by the intact ipsilateral ear shortly after denervation (Figure 7). Although the ipsilateral ear competed for representational salience with the denervated contralateral ear, its presence nevertheless facilitated recovery of function; sound-evoked activity was completely absent 7 days after bilateral denervation and exhibited a comparatively modest recovery of spike rate decoding when tested at the 30 day time point (Figure 8). There is extensive in vivo evidence for compensatory central gain increases following peripheral insult in a variety of hearing loss models, though recovery has never been demonstrated from an afferent loss this specific or extreme (Auerbach et al., 2014; Cheung et al., 2009; Qiu et al., 2000; Schuknecht and Woellner, 1953; Wake et al., 1996).

Whether as a consequence of acute trauma or normal aging, SGNs degenerate and the bandwidth of information transmitted from the cochlea to the brain decreases. Neuropathy begins as a loss of synaptic contacts between SGNs and IHCs. With time, the pathology extends to include the retraction of peripheral SGN processes and, ultimately, the death of SGNs at a rate of approximately 1,000 per decade in humans (Makary et al., 2011). A "moderate" loss of cochlear afferent synapses (~50%) has been associated with a so-called "hidden hearing loss" that manifests as an inability to properly encode temporal envelope cues and a reduction in ABR amplitude without a commensurate shift in ABR or audiometric thresholds (Bharadwaj et al., 2015; Kujawa and Liberman, 2009).

More extreme afferent loss can underlie ANSD, characterized by the absence of an ABR, profound temporal processing deficits, and an inability to extract intelligible information from speech, even when audibility thresholds are relatively normal (Starr et al., 1996; Zeng et al., 2005). Our mouse model captures each of the defining features of ANSD observed in human patients. However, our findings challenge the widespread assumption that preservation of thresholds and intensity discrimination despite devastating impairments in temporal processing and speech reception must be attributable to a dys-synchronization of spike timing in auditory nerve fibers (Berlin et al., 2010; Zeng et al., 2005). Auditory nerve dys-synchronization has never been specifically or directly demonstrated in ANSD. Instead, our findings point toward an alternative etiology: a compensatory plasticity at higher stages of the CNS following profound afferent degeneration that can support the recovery of rate coding for rudimentary sound features, but not precise temporal firing patterns.

Auditory brainstem neurons can encode fluctuations in the acoustic source signal on the order of tens of microseconds while maintaining sustained firing rates above 1 kHz. This remarkable high speed processing is supported by unique synaptic architecture, inhibitory circuitry, and biophysical specializations not found at higher auditory centers (Lu et al., 2008; Mathews et al., 2010; McGinley et al., 2012). What higher auditory neurons lack in specialized high-speed decoding, they make up for in intrinsic and synaptic properties that maintain plasticity well into adulthood. The remarkable plasticity of the adult ACtx is derived from several characteristics not observed in most lower auditory nuclei: (1) massive convergence, such that a given ACtx neuron receives subthreshold input from a wide range of sound frequencies and afferent sources (Chen et al., 2011; Hackett et al., 2011), (2) co-tuned, but temporally offset synaptic excitation and inhibition that prevents all but the largest and fastest subthreshold inputs from eliciting action potentials (Tan et al., 2004; Wehr and Zador, 2003; Wu et al., 2008), (3) dense input from neuromodulatory nuclei that can temporarily disable inhibitory control and rapidly rescale the strength of latent inputs through Hebbian processes (Froemke et al., 2007, 2013; Letzkus et al., 2011), and (4) homeostatic mechanisms that maintain neural activity near a set point (Kotak et al., 2005; Seybold et al., 2012; Yang et al., 2011).

In this light, the compensatory gain control described here may represent the default homeostatic response of higher auditory circuits deprived of bottom-up afferent drive. The intrinsic gain enhancement may facilitate a rapid and complete recovery of sensitivity to diminished afferent inputs, but this recovery does not extend to—and indeed may even interfere with—precise temporal coding. Moreover, the increased gain needed to restore activity levels to a homeostatic set point can push cortical networks toward unstable states of heightened excitability that may underlie tinnitus and hyperacusis (Auerbach et al., 2014). Further recovery in temporal processing fidelity (Engineer et al., 2015; Zhou and Merzenich, 2009) and complex sound discrimination (Whitton et al., 2014) may be possible in the sensory impaired if these default compensatory processes are augmented by sensory rehabilitation paradigms that engage untapped Hebbian plasticity mechanisms.

EXPERIMENTAL PROCEDURES

Many additional details for each of the subheadings below can be found in the Supplemental Information.

Animals and Cochlear Denervation

All procedures were approved by the Animal Care and Use Committee at the Massachusetts Eye and Ear Infirmary and followed guidelines established by the NIH for the care and use of laboratory animals. Unilateral cochlear denervation was performed on 25 male CBA/CaJ mice, 8–10 weeks old. Bilateral denervation experiments were carried out on an additional six adult male mice (B6129 hybrid background). Selective elimination of Type-I SGNs was achieved by applying a 1 mM solution of ouabain octahydrate (Sigma) and sterile water to the round window niche, as described previously (Lang et al., 2005; Yuan et al., 2014).

Measurements of Cochlear Anatomy and Physiology

Lengths of cochlear whole mounts were measured and converted to cochlear frequency. Confocal z stacks were obtained in the IHC area. ABR stimuli were 5-ms tone pips (8, 16, and 32 kHz pure tones, from 20–80 dB SPL in 5 dB steps). The 2f1-f2 distortion product otoacoustic emission (DPOAE) SPL was recorded in the ear canal using primary tones with a frequency ratio of 1.2, with the level of the f2 primary set to be 10 dB less than f1 level, incremented together in 5 dB steps.

Behavioral Experiments

For acoustic startle testing, mice were fit with an earplug in one ear and placed into a small cage resting atop a piezoelectric sensor plate. An 8 kHz tone (70–110 dB SPL) was presented at varying time intervals from an overhead speaker. Startle response amplitude was measured as the maximum peak-to-peak voltage of the force plate signal shortly after sound presentation. Conscious perception of tones was measured with an auditory avoidance task (Guo et al., 2015). Unilaterally plugged mice crossed from one side of an acoustically transparent rectangular enclosure to another upon the presentation of an 8 kHz pure tone (10–90 dB SPL) in order to avoid a weak foot shock (0.3–0.5 mA).

Chronic Recording Probe Implantation

For unilateral denervation experiments, mice were implanted with multichannel silicon probes in ACtx and IC (177 μm^2 contact area; NeuroNexus Technologies). For bilateral denervation experiments, mice were implanted with a microdrive array containing four independently moveable tetrodes (Neuralynx). Tetrodes were constructed by twisting together four nichrome wires (12.5 μm in diameter, Stablohm 650 wire, California Fine Wire) and then electroplating each microwire with gold to reach an impedance of 0.5–1 MΩ.

Neurophysiology Data Collection

For unilateral denervation experiments, mice were placed in a small, acoustically transparent chamber just large enough for their body. Recording was paused if the mouse closed its eyes, reared, or moved its head from the target

position. For bilateral denervation experiments, recordings were made under head restraint. Multiunit spikes were detected as threshold-crossing events using an objective, adaptive thresholding procedure in which the threshold was set to 3.5 SDs from the mean of a 10 s running average.

Stimuli and Data Analysis

Stimulus-driven sites were identified by binning the PSTH at 10 ms resolution and determining if a single bin in the stimulus-evoked period (the duration of the stimulus plus 50 ms) was more than three SDs above the spontaneous firing rate distribution. FRAs were delineated from 990 pseudorandomly presented tone pips. Rate-level function gain and threshold were determined from a two-tailed, six parameter Gaussian fit. Synchronization was measured using frequency-modulated chirps (1 ms in duration spanning 4–64 kHz presented at rates ranging from 1–300 Hz). Speech tokens were synthesized from 12 consonant-vowel-consonants shifted by four octaves without temporal distortion. PSTH classifier models compare the ensemble single trial spike train evoked by a given stimulus to ensemble spike trains responses elicited by all other stimuli. The single trial response is classified to the stimulus to which the Euclidean distance is smallest. For sound level classification, the margin of error for correct classification was ± 5 dB from the actual presented stimulus (Figures 3 and 8).

SUPPLEMENTAL INFORMATION

Supplemental Information includes Supplemental Experimental Procedures, six figures, and one table and can be found with this article online at http://dx.doi.org/10.1016/j.neuron.2015.12.041.

AUTHOR CONTRIBUTIONS

A.R.C. and J.R. performed all experiments. A.R.C. analyzed all data. A.R.C. and M.C.L. performed cochlear histopathology experiments. J.P.W. recorded and synthesized speech tokens. Y.Y., J.P.W., and D.B.P. performed pilot experiments. A.S.E. provided guidance and reagents for ouabain application. A.R.C. and D.B.P. wrote the manuscript.

ACKNOWLEDGMENTS

We thank Mark Liu and Krupa Shukla for assisting with behavioral measurements, Leslie Liberman for preparing cochlear whole mount sections, and Ken Hancock for programming assistance. This work was supported by R01 DC009836 (D.B.P.), R01 DC007174 (A.S.E.), R01 DC 00188 (M.C.L.), P30 05209 (M.C.L.), a research grant from Autifony Therapeutics (D.B.P.), and the Lauer Tinnitus Research Center (M.C.L. and D.B.P.).

Received: August 10, 2015
Revised: November 5, 2015
Accepted: December 16, 2015
Published: January 28, 2016

REFERENCES

Atencio, C.A., Sharpee, T.O., and Schreiner, C.E. (2012). Receptive field dimensionality increases from the auditory midbrain to cortex. J. Neurophysiol. *107*, 2594–2603.

Atiani, S., Elhilali, M., David, S.V., Fritz, J.B., and Shamma, S.A. (2009). Task difficulty and performance induce diverse adaptive patterns in gain and shape of primary auditory cortical receptive fields. Neuron *61*, 467–480.

Auerbach, B.D., Rodrigues, P.V., and Salvi, R.J. (2014). Central gain control in tinnitus and hyperacusis. Front. Neurol. *5*, 206.

Ayala, Y.A., Pérez-González, D., Duque, D., Nelken, I., and Malmierca, M.S. (2013). Frequency discrimination and stimulus deviance in the inferior colliculus and cochlear nucleus. Front. Neural Circuits *6*, 119.

Berlin, C.I., Hood, L.J., Morlet, T., Wilensky, D., Li, L., Mattingly, K.R., Taylor-Jeanfreau, J., Keats, B.J.B., John, P.S., Montgomery, E., et al. (2010). Multi-site diagnosis and management of 260 patients with auditory neuropathy/dys-synchrony (auditory neuropathy spectrum disorder). Int. J. Audiol. *49*, 30–43.

Bharadwaj, H.M., Masud, S., Mehraei, G., Verhulst, S., and Shinn-Cunningham, B.G. (2015). Individual differences reveal correlates of hidden hearing deficits. J. Neurosci. *35*, 2161–2172.

Chen, X., Leischner, U., Rochefort, N.L., Nelken, I., and Konnerth, A. (2011). Functional mapping of single spines in cortical neurons in vivo. Nature *475*, 501–505.

Cheung, S.W., Bonham, B.H., Schreiner, C.E., Godey, B., and Copenhaver, D.A. (2009). Realignment of interaural cortical maps in asymmetric hearing loss. J. Neurosci. *29*, 7065–7078.

Dean, I., Robinson, B.L., Harper, N.S., and McAlpine, D. (2008). Rapid neural adaptation to sound level statistics. J. Neurosci. *28*, 6430–6438.

Diamond, D.M., and Weinberger, N.M. (1986). Classical conditioning rapidly induces specific changes in frequency receptive fields of single neurons in secondary and ventral ectosylvian auditory cortical fields. Brain Res. *372*, 357–360.

Ding, N., and Simon, J.Z. (2012). Emergence of neural encoding of auditory objects while listening to competing speakers. Proc. Natl. Acad. Sci. USA *109*, 11854–11859.

Engineer, C.T., Rahebi, K.C., Buell, E.P., Fink, M.K., and Kilgard, M.P. (2015). Speech training alters consonant and vowel responses in multiple auditory cortex fields. Behav. Brain Res. *287*, 256–264.

Froemke, R.C., Merzenich, M.M., and Schreiner, C.E. (2007). A synaptic memory trace for cortical receptive field plasticity. Nature *450*, 425–429.

Froemke, R.C., Carcea, I., Barker, A.J., Yuan, K., Seybold, B.A., Martins, A.R.O., Zaika, N., Bernstein, H., Wachs, M., Levis, P.A., et al. (2013). Long-term modification of cortical synapses improves sensory perception. Nat. Neurosci. *16*, 79–88.

Glazewski, S., Benedetti, B.L., and Barth, A.L. (2007). Ipsilateral whiskers suppress experience-dependent plasticity in the barrel cortex. J. Neurosci. *27*, 3910–3920.

Guo, W., Hight, A.E., Chen, J.X., Klapoetke, N.C., Hancock, K.E., Shinn-Cunningham, B.G., Boyden, E.S., Lee, D.J., and Polley, D.B. (2015). Hearing the light: neural and perceptual encoding of optogenetic stimulation in the central auditory pathway. Sci. Rep. *5*, 10319.

Gutschalk, A., Micheyl, C., and Oxenham, A.J. (2008). Neural correlates of auditory perceptual awareness under informational masking. PLoS Biol. *6*, e138.

Hackett, T.A., Barkat, T.R., O'Brien, B.M.J., Hensch, T.K., and Polley, D.B. (2011). Linking topography to tonotopy in the mouse auditory thalamocortical circuit. J. Neurosci. *31*, 2983–2995.

Keck, T., Mrsic-Flogel, T.D., Vaz Afonso, M., Eysel, U.T., Bonhoeffer, T., and Hübener, M. (2008). Massive restructuring of neuronal circuits during functional reorganization of adult visual cortex. Nat. Neurosci. *11*, 1162–1167.

Kotak, V.C., Fujisawa, S., Lee, F.A., Karthikeyan, O., Aoki, C., and Sanes, D.H. (2005). Hearing loss raises excitability in the auditory cortex. J. Neurosci. *25*, 3908–3918.

Kral, A., Hubka, P., Heid, S., and Tillein, J. (2013). Single-sided deafness leads to unilateral aural preference within an early sensitive period. Brain *136*, 180–193.

Kujawa, S.G., and Liberman, M.C. (2009). Adding insult to injury: cochlear nerve degeneration after "temporary" noise-induced hearing loss. J. Neurosci. *29*, 14077–14085.

Lang, H., Schulte, B.A., and Schmiedt, R.A. (2005). Ouabain induces apoptotic cell death in type I spiral ganglion neurons, but not type II neurons. J. Assoc. Res. Otolaryngol. *6*, 63–74.

Letzkus, J.J., Wolff, S.B.E., Meyer, E.M.M., Tovote, P., Courtin, J., Herry, C., and Lüthi, A. (2011). A disinhibitory microcircuit for associative fear learning in the auditory cortex. Nature *480*, 331–335.

Lu, T., Rubio, M.E., and Trussell, L.O. (2008). Glycinergic transmission shaped by the corelease of GABA in a mammalian auditory synapse. Neuron *57*, 524–535.

Makary, C.A., Shin, J., Kujawa, S.G., Liberman, M.C., and Merchant, S.N. (2011). Age-related primary cochlear neuronal degeneration in human temporal bones. J. Assoc. Res. Otolaryngol. *12*, 711–717.

Mathews, P.J., Jercog, P.E., Rinzel, J., Scott, L.L., and Golding, N.L. (2010). Control of submillisecond synaptic timing in binaural coincidence detectors by K(v)1 channels. Nat. Neurosci. *13*, 601–609.

McGinley, M.J., Liberman, M.C., Bal, R., and Oertel, D. (2012). Generating synchrony from the asynchronous: compensation for cochlear traveling wave delays by the dendrites of individual brainstem neurons. J. Neurosci. *32*, 9301–9311.

Merzenich, M.M., Nelson, R.J., Stryker, M.P., Cynader, M.S., Schoppmann, A., and Zook, J.M. (1984). Somatosensory cortical map changes following digit amputation in adult monkeys. J. Comp. Neurol. *224*, 591–605.

Mesgarani, N., and Chang, E.F. (2012). Selective cortical representation of attended speaker in multi-talker speech perception. Nature *485*, 233–236.

Moore, B.C.J. (2007). Cochlear Hearing Loss: Physiological, Psychological and Technical Issues (John Wiley & Sons).

Mowery, T.M., Kotak, V.C., and Sanes, D.H. (2015). Transient hearing loss within a critical period causes persistent changes to cellular properties in adult auditory cortex. Cereb. Cortex *25*, 2083–2094.

Pasley, B.N., David, S.V., Mesgarani, N., Flinker, A., Shamma, S.A., Crone, N.E., Knight, R.T., and Chang, E.F. (2012). Reconstructing speech from human auditory cortex. PLoS Biol. *10*, e1001251.

Qiu, C., Salvi, R., Ding, D., and Burkard, R. (2000). Inner hair cell loss leads to enhanced response amplitudes in auditory cortex of unanesthetized chinchillas: evidence for increased system gain. Hear. Res. *139*, 153–171.

Rabinowitz, N.C., Willmore, B.D.B., Schnupp, J.W.H., and King, A.J. (2011). Contrast gain control in auditory cortex. Neuron *70*, 1178–1191.

Rabinowitz, N.C., Willmore, B.D.B., King, A.J., and Schnupp, J.W.H. (2013). Constructing noise-invariant representations of sound in the auditory pathway. PLoS Biol. *11*, e1001710.

Reed, A.C., Centanni, T.M., Borland, M.S., Matney, C.J., Engineer, C.T., and Kilgard, M.P. (2014). Behavioral and neural discrimination of speech sounds after moderate or intense noise exposure in rats. Ear Hear. *35*, e248–e261.

Robertson, D., and Irvine, D.R. (1989). Plasticity of frequency organization in auditory cortex of guinea pigs with partial unilateral deafness. J. Comp. Neurol. *282*, 456–471.

Scholl, B., and Wehr, M. (2008). Disruption of balanced cortical excitation and inhibition by acoustic trauma. J. Neurophysiol. *100*, 646–656.

Schuknecht, H.F., and Woellner, R.C. (1953). Hearing losses following partial section of the cochlear nerve. Laryngoscope *63*, 441–465.

Seybold, B.A., Stanco, A., Cho, K.K.A., Potter, G.B., Kim, C., Sohal, V.S., Rubenstein, J.L.R., and Schreiner, C.E. (2012). Chronic reduction in inhibition reduces receptive field size in mouse auditory cortex. Proc. Natl. Acad. Sci. USA *109*, 13829–13834.

Starr, A., Picton, T.W., Sininger, Y., Hood, L.J., and Berlin, C.I. (1996). Auditory neuropathy. Brain *119*, 741–753.

Tan, A.Y.Y., Zhang, L.I., Merzenich, M.M., and Schreiner, C.E. (2004). Tone-evoked excitatory and inhibitory synaptic conductances of primary auditory cortex neurons. J. Neurophysiol. *92*, 630–643.

Tomita, M., Noreña, A.J., and Eggermont, J.J. (2004). Effects of an acute acoustic trauma on the representation of a voice onset time continuum in cat primary auditory cortex. Hear. Res. *193*, 39–50.

Wake, M., Takeno, S., Mount, R.J., and Harrison, R.V. (1996). Recording from the inferior colliculus following cochlear inner hair cell damage. Acta Otolaryngol. *116*, 714–720.

Wang, X., Lu, T., Bendor, D., and Bartlett, E. (2008). Neural coding of temporal information in auditory thalamus and cortex. Neuroscience *157*, 484–494.

Wehr, M., and Zador, A.M. (2003). Balanced inhibition underlies tuning and sharpens spike timing in auditory cortex. Nature *426*, 442–446.

Whitton, J.P., Hancock, K.E., and Polley, D.B. (2014). Immersive audiomotor game play enhances neural and perceptual salience of weak signals in noise. Proc. Natl. Acad. Sci. USA *111*, E2606–E2615.

Wu, G.K., Arbuckle, R., Liu, B.H., Tao, H.W., and Zhang, L.I. (2008). Lateral sharpening of cortical frequency tuning by approximately balanced inhibition. Neuron *58*, 132–143.

Yang, S., Weiner, B.D., Zhang, L.S., Cho, S.-J., and Bao, S. (2011). Homeostatic plasticity drives tinnitus perception in an animal model. Proc. Natl. Acad. Sci. USA *108*, 14974–14979.

Yang, S., Su, W., and Bao, S. (2012). Long-term, but not transient, threshold shifts alter the morphology and increase the excitability of cortical pyramidal neurons. J. Neurophysiol. *108*, 1567–1574.

Yaron, A., Hershenhoren, I., and Nelken, I. (2012). Sensitivity to complex statistical regularities in rat auditory cortex. Neuron *76*, 603–615.

Yin, P., Johnson, J.S., O'Connor, K.N., and Sutter, M.L. (2011). Coding of amplitude modulation in primary auditory cortex. J. Neurophysiol. *105*, 582–600.

Yuan, Y., Shi, F., Yin, Y., Tong, M., Lang, H., Polley, D.B., Liberman, M.C., and Edge, A.S.B. (2014). Ouabain-induced cochlear nerve degeneration: synaptic loss and plasticity in a mouse model of auditory neuropathy. J. Assoc. Res. Otolaryngol. *15*, 31–43.

Zeng, F.-G., Kong, Y.-Y., Michalewski, H.J., and Starr, A. (2005). Perceptual consequences of disrupted auditory nerve activity. J. Neurophysiol. *93*, 3050–3063.

Zhou, X., and Merzenich, M.M. (2009). Developmentally degraded cortical temporal processing restored by training. Nat. Neurosci. *12*, 26–28.

Zion Golumbic, E.M., Ding, N., Bickel, S., Lakatos, P., Schevon, C.A., McKhann, G.M., Goodman, R.R., Emerson, R., Mehta, A.D., Simon, J.Z., et al. (2013). Mechanisms underlying selective neuronal tracking of attended speech at a "cocktail party". Neuron *77*, 980–991.